Mapping Crop Types across Mixed Single- and Double-Cropping Systems in Brazil Using Satellite Time-Series Data and Machine Learning

Shoki Shimada [1*], and Kei Oyoshi [1]

[1]Japan Aerospace Exploration Agency (JAXA), Tsukuba 305-8505, Japan

*shimada.shohki@jaxa.jp

Abstract *Brazil, a major global agricultural exporter, plays a key role in the food supply chain, making accurate monitoring of its crop production essential for food security. Due to its vast area, satellite remote sensing is crucial for timely and cost-effective crop mapping, particularly given Brazil's mix of double and single cropping systems, such as soybean-corn or soybean-cotton rotations and long-cycle crops like sugarcane. This study maps five key crops—soybean, corn, cotton, sugarcane, and other grains (sorghum and millet)—using Geen Cholophill Vgetation Index (GCVI) time series data from Landsat and Sentinel-2 between September 2023 and August 2024, and other satellite data sources including the ALOS-2 L-band SAR data. The data were smoothed using the Harmonic ANalysis of Time Series (HANTS) algorithm in Google Earth Engine, and crop cycles were segmented through peak detection. Skewed normal distributions were fitted to each season's phenology, and their parameters were used as input features for a Random Forest model to classify crop types in central Brazil. The model achieved an overall accuracy of 0.936, and municipality-level estimates for soybean, corn, cotton, and sugarcane showed strong agreement with official statistics, with R^2 values of 0.95, 0.94, 0.96, and 0.85, respectively. These results demonstrate the method's effectiveness for accurate and timely crop mapping in regions with complex agricultural practices.*

Keywords: *Phenology, Random Forest, Food Security, Remote Sensing*

1. Introduction

The global population has continued to increase over the past several decades, surpassing 8 billion in 2024, more than double that of 60 years ago (WorldMeter, n.d.). This rapid growth has driven a substantial rise in global food demand, placing increasing pressure on agricultural systems. Advances in modern agricultural technologies have enabled several countries, including the United States, Canada, Australia, Brazil, and Russia, to emerge as major exporters of staple crops. The crop production status of these countries directly influences global food prices and trade stability, making accurate information on agricultural production essential for maintaining reliable food supplies in importing nations such as Japan.

Satellite remote sensing has become a central tool for monitoring crop production at regional to global scales (Khosravi, 2025). Its repeated observation schedules, wide spatial coverage, and diverse sensing capabilities, including both optical and radar sensors, enable timely and consistent assessments of crop patterns and growth conditions. Since individual crops exhibit distinct seasonal growth dynamics, referred to as crop phenology, the use of

multi-temporal satellite data facilitates the quantitative characterization of phenological patterns. Combined with advances in machine learning, satellite-based time-series analyses have significantly improved the ability to generate accurate and up-to-date crop maps.

Extensive efforts have been made to produce high-resolution crop maps using satellite observations at national and continental scales. The Cropland Data Layer (CDL), developed by the U.S. Department of Agriculture (USDA), integrates multi-sensor data and field samples to classify up to 255 crop types across the continental United States (Boryan et al., 2011; Wang et al., 2020). Similar initiatives include the Agriculture and Agri-Food Canada (AAFC) crop inventory (Earth Observation Team of the Science and Technology Branch, n.d.), European countries (d'Andrimont et al., 2021; Schneider et al., 2023), and MapBiomas in Brazil (Souza et al., 2020). The land-cover map of Japan includes rice-paddy category (Sota et al., 2022). These products often employ Random Forest and other machine learning models (Tatsumi et al., 2015; Wang et al., 2019), leveraging input features from optical reflectance, radar backscatter, and time-series metrics, and have demonstrated high classification accuracies in large-scale crop-type mapping.

Despite these advances, significant challenges remain in accurately mapping multi-cropping systems, particularly in tropical and subtropical regions where double- and triple-cropping practices are widespread. Conventional annual crop maps, which assign a single crop label to each pixel, often fail to represent the actual cropping practices in these areas. Some studies have addressed this limitation by dividing the year into separate growing seasons (Ajadi et al., 2021; Pazhanivelan et al., 2025). However, this approach has inherent drawbacks, as the timing of planting and harvesting could vary among farmers, making it difficult to establish universal thresholds for segmenting crop cycles. Fourier-transform based approach was taken to classify double-cropping systems to distinguish wheat-maize, wheat-cotton, cotton, and maize (Mingwei et al., 2008). It requires the settings of multiple cropping patterns beforehand, complicating the dataset preparations. Furthermore, in landscapes where single- and double-cropping coexist, applying fixed thresholds can lead to misclassification and reduced accuracy.

To address these challenges, pixel-level time-series analyses are needed to directly detect and parameterize individual crop-growing segments within a year without imposing predefined temporal thresholds. A previous study in Saga Prefecture, Japan, demonstrated that pixel-based modeling of phenological curves enables accurate identification of single, double, and even triple cropping systems, resulting in high-accuracy multi-season crop maps (Shimada & Oyoshi, 2025).

Building on this concept, the objective of this study is to develop and apply a phenology-based, pixel-level crop mapping framework to central Brazil, one of the world's most important agricultural regions. This area is characterized by extensive double-cropping practices, including soybean-corn and soybean-cotton rotations, which are poorly represented in existing annual land-cover products such as MapBiomas (Souza et al., 2020). By integrating multi-sensor satellite time-series data with phenology-driven parameterization and machine learning, this study aims to generate multi-season crop maps and evaluate their consistency with both existing products and municipality-level crop statistics, providing a robust approach for monitoring agricultural dynamics in regions with complex cropping systems.

2. Methodology

2.1 Study area and the target crops

The study area covers nine central states of Brazil: Bahia, Goiás, Distrito Federal (the capital, Brasília), Mato Grosso, Mato Grosso do Sul, Minas Gerais, São Paulo, Tocantins, and Piauí, which are primarily located within the Cerrado region. The Cerrado is one of the most important agricultural zones in Brazil. Historically a semi-arid savanna with limited agricultural activity, it has transformed into a major crop production area, particularly for soybean, for which Brazil holds the largest export share globally. This study analyzes crop patterns during the September 2023 to September 2024 growing season.

Our target crops were soybean, corn, cotton, sugarcane, and other grains (sorghum and millet), which are considered important for agricultural production in the region based on relevant literature. According to the crop calendar provided by the USDA Foreign Agricultural Service (FAS), soybean is typically planted from September to December and harvested from January to June. Second-season corn and cotton are generally planted in January and harvested between May and September. Sorghum is planted from October to the following February and harvested between May and August. In contrast, sugarcane requires a much longer growing period of approximately 12 to 18 months, distinguishing it from other temporary crops. For reference data, we prepared field samples for each crop by utilizing ground-level imagery available from Google Street View (GSV).

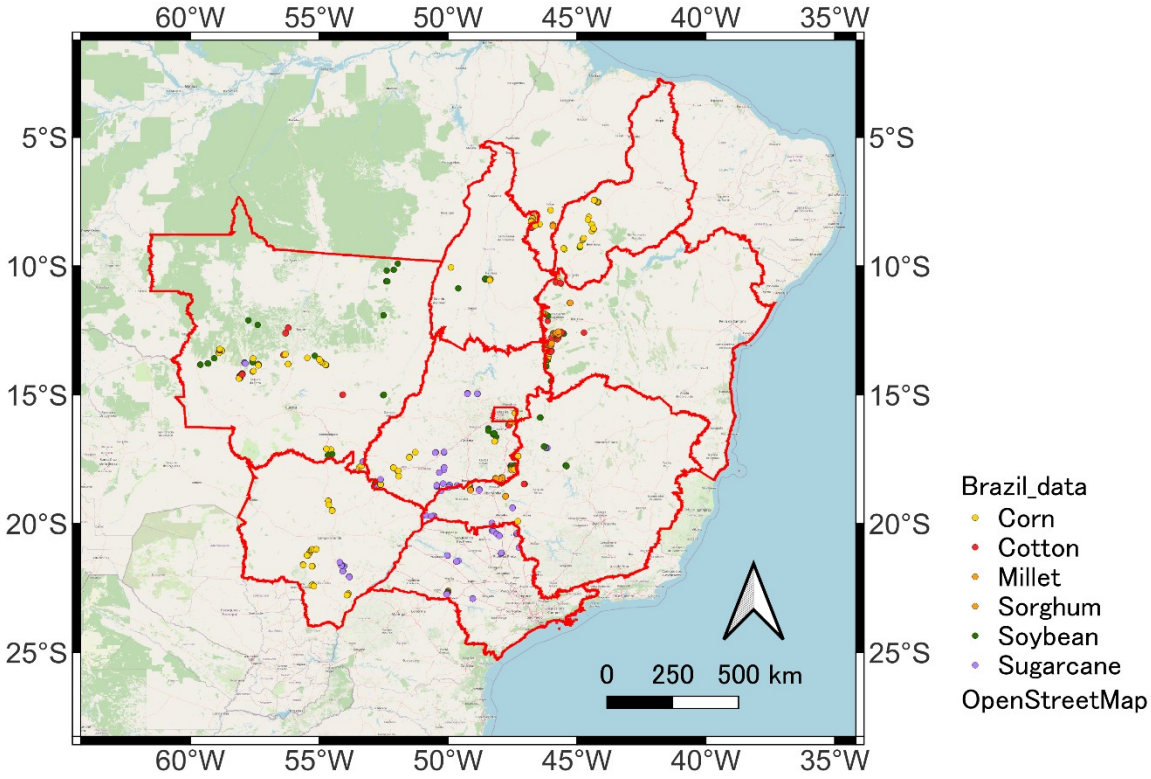

Figure. 1 The distribution of the crop-sample points by using the GSV images.

2.2 Satellite data

The phenological features of the target crops were analyzed using time-series data from Sentinel-2 and Landsat-8/9. These satellites are equipped with multi-spectral, medium-resolution optical sensors that provide data at spatial resolutions ranging from 10 m to 60 m. The imagery was pre-processed on the Google Earth Engine (GEE) platform to remove clouds, cloud shadows, and other low-quality pixels. We calculated the Green Chlorophyll Vegetation Index (GCVI) to characterize the phenological patterns of crop growth and harvest. GCVI is defined as the ratio between near-infrared (NIR) and green reflectance, as shown in equation (1). Compared with other vegetation indices, such as NDVI, GCVI offers a higher saturation threshold under high leaf area index (LAI) conditions.

$$\mathbf{GCVI} = \frac{\boldsymbol{NIR}}{\boldsymbol{Green}} - \mathbf{1} \ldots (\mathbf{1})$$

The raw GCVI dataset contains noisy observations due to variations in satellite acquisitions. Therefore, a HANTS (Harmonic ANalysis of Time Series) approach was applied to obtain a clearer representation of crop growth patterns. The details of the HANTS-based noise

reduction on GCVI time-series are described in the literature (Shimada & Oyoshi, 2025).

In addition to the GCVI time-series data, other remote-sensing datasets were utilized to better characterize the differences among crops. Topographic features (elevation and slope) were derived from the AW3D 30 m global DSM dataset, with slope calculated using the `ee.Terrain.Slope` function in GEE. In addition to the optical features, we incorporated Level-2.2 ALOS-2 ScanSAR datasets. Based on the crop-growing calendar in the target region, a wet growing season (September to the following April) and a dry growing season (February to August) were defined. The statistical mean and standard deviation of the ALOS-2 HH and HV polarizations were calculated for each season, resulting in a total of eight ALOS-2 statistical variables (2 polarizations × 2 seasons × 2 statistics) per year. Both the phenology-related data and the additional satellite-derived features were extracted at each crop-sample point at 30 m spatial resolution for dataset preparation. However, due to computational limitations, the final crop maps were generated at 250 m spatial resolution.

2.3 Time-series segmentation and crop-phenology parameterization

Based on the GCVI time-series, the relevant crop-phenology patterns were parameterized. The skewed-normal distribution function has been shown to be effective for parameterizing non-symmetric but near bell-shaped GCVI curves in double-cropping regions of Japan. We adopted the same strategy to address the mixed single- and double-cropping patterns in the target region. The parameterization workflow consists of three steps: (1) applying a HANTS-based curve fit to the raw GCVI time series, (2) performing peak detection and segmenting crop-growing periods on the smoothed GCVI curves, and (3) fitting the skewed-normal distribution function to each segmented time-series data. The `scipy.signal.find_peaks` algorithm was used to identify peaks in the GCVI time-series. The maximum number of peaks was limited to three, assuming that practical crop cycles would not exceed triple cropping. Each crop-growing segment was defined by a detected peak and the local minima before and after the peak. Within each segment, the skewed-normal distribution function, defined by equation (2), was fitted using the `scipy.optimize.curve_fit` algorithm. There are five parameters in total: four parameters from the fitted skewed-normal distribution function and the maximum value of the function, expressed by equation (3). Here, x represents the relative time from 0 (September) to 1 (next August).

$$h(x) = k\frac{2}{\omega}\phi\left(\frac{x-\xi}{\omega}\right)\Phi\left(\alpha\left(\frac{x-\xi}{\omega}\right)\right) \ldots (2)$$

$$A = \max\big(h(x)\big) \ldots (3)$$

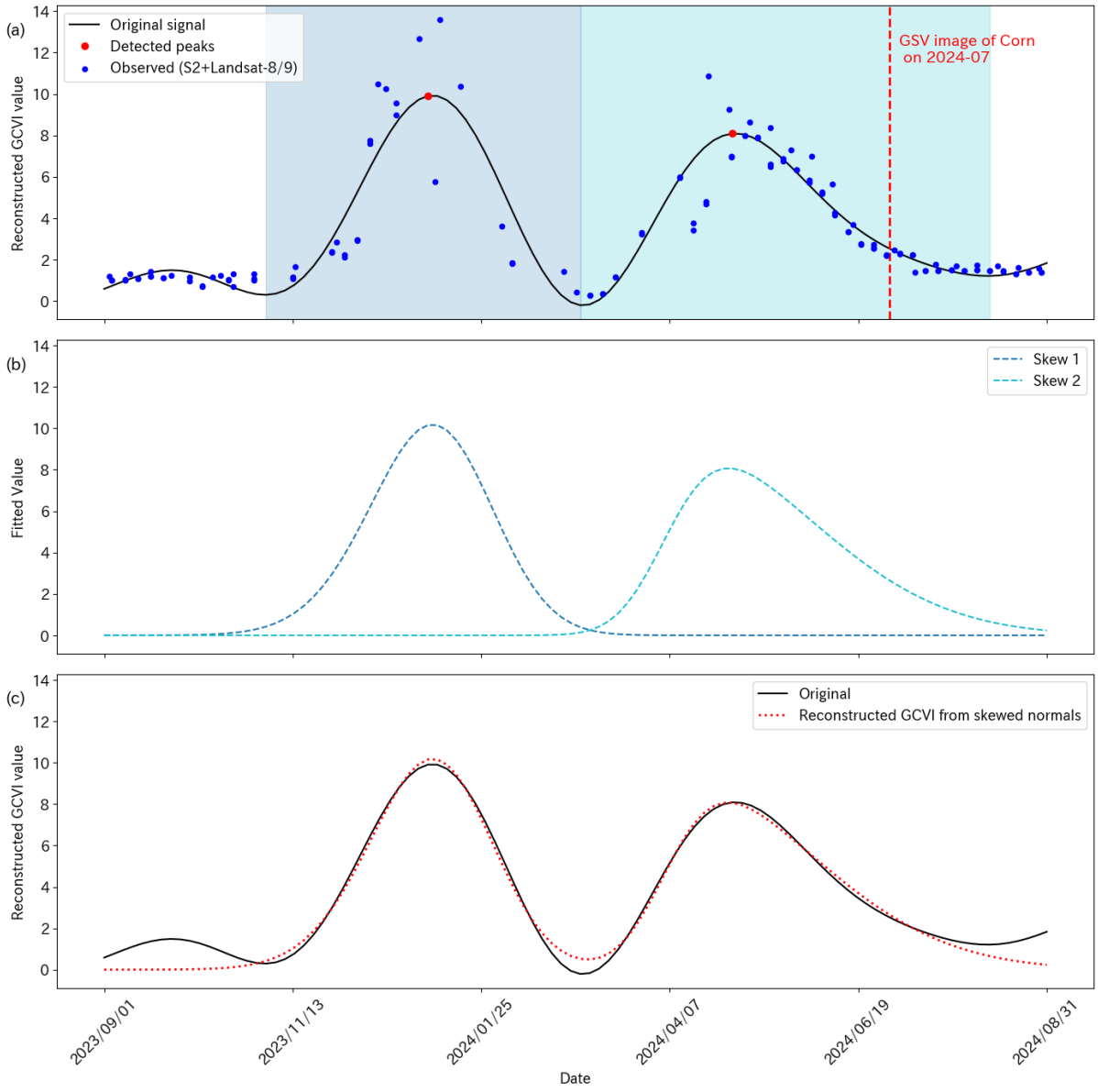

Figure.2 The time-series segmentation and crop-phenology parametrization with skewed-normal distribution functions. (a) The raw-GCVI time-series, HANTS-based smoothed time-series, and the detected peaks. (b) The fitted skewed normal distribution function on each segment. (c) Comparison between the smoothed GCVI curve, and the reconstructed curve by summing the individual crop-growing phenological curve.

2.4 Crop-mapping with a machine-learning model

A crop-mapping model was established using five crop-phenology-related parameters extracted from the GCVI time-series, two topographic features (elevation and slope), and eight ALOS-2-derived statistical variables. We employed a Random Forest model, an ensemble learning method based on decision tree algorithms. The model generates robust predictions by training multiple weak decision trees with different configurations and aggregating their results through majority voting. The key model parameters were set as follows: `n_estimators` = 300 and `class_weight` = "balanced", while other parameters were kept at their default values.

The input dataset was split into training and validation subsets at a 75:25 ratio. Model performance was evaluated on the validation dataset using four accuracy metrics: overall accuracy, Cohen's kappa coefficient, precision, and recall. The trained model was then applied to the entire cropland area of the target region at 250 m spatial resolution to produce a crop map for the September 2023 to September 2024 season. Crop masks were derived from the Dynamic World land-cover dataset, which was preprocessed within the study period to determine the dominant ("mode") land-cover type at each pixel. The resulting crop map contains three bands, each corresponding to a distinct crop-growing segment derived from the GCVI time-series. For locations with only single- or double-cropping cycles, the unused bands were left blank.

2.5 Validating crop-map result with crop-statistics

The produced crop map was validated against the official crop statistics prepared by the Instituto Brasileiro de Geografia e Estatística (IBGE), the Brazilian Institute of Geography and Statistics. We used the 2023 municipality-level crop area statistics available from the official website of the target states (IBGE, 2023).

The satellite-derived crop maps were first combined into an annual crop map. For example, corn may be cultivated in either the first season or the second season following soybean planting. These pixels were merged, and the union of the three crop-growing segments was calculated to produce the overall crop map for the study period. To estimate crop-growing areas within each municipality, the proportion of the area occupied by each target crop was calculated by dividing the total number of crop-specific pixels (e.g., soybean) by the total

number of pixels. This proportion was then multiplied by the total area of the municipality to obtain the estimated crop area. Finally, the estimated crop area statistics were compared with the official planted-area statistics to evaluate the reliability of the satellite-derived crop map.

3. Results and Discussions

3.1 Extracted crop-phenology pattern and the differences in the satellite-derived parameters

The extracted crop-phenology patterns from the GCVI time-series data are shown in Figure 3. Each crop exhibited a distinct pattern related to differences in planting and harvesting seasons as well as overall growth dynamics. Soybean typically began its growing period around November, ended in April, and reached its maximum growth around January, which aligns well with the established crop-growing calendar in Brazil. Sugarcane showed the longest crop-growing period, lasting almost a full year, reflecting the 12 to 18 months required for its maturation and harvest.

The remaining three crops—corn, cotton, and other grains—showed phenological peaks around May, corresponding to the drier season in the target region. These patterns are consistent with the common double-cropping practice, in which corn, cotton, or cover crops (grains) are planted after soybean harvest. Notable differences were also observed among these crops. For example, the other-grains category showed a lower maximum GCVI value compared to corn and cotton, likely due to shorter crop height and less dense canopy structure. Corn and cotton can be further distinguished by the length and symmetry of their growing periods, with cotton exhibiting a longer growth cycle, while corn displays a more asymmetric phenological curve.

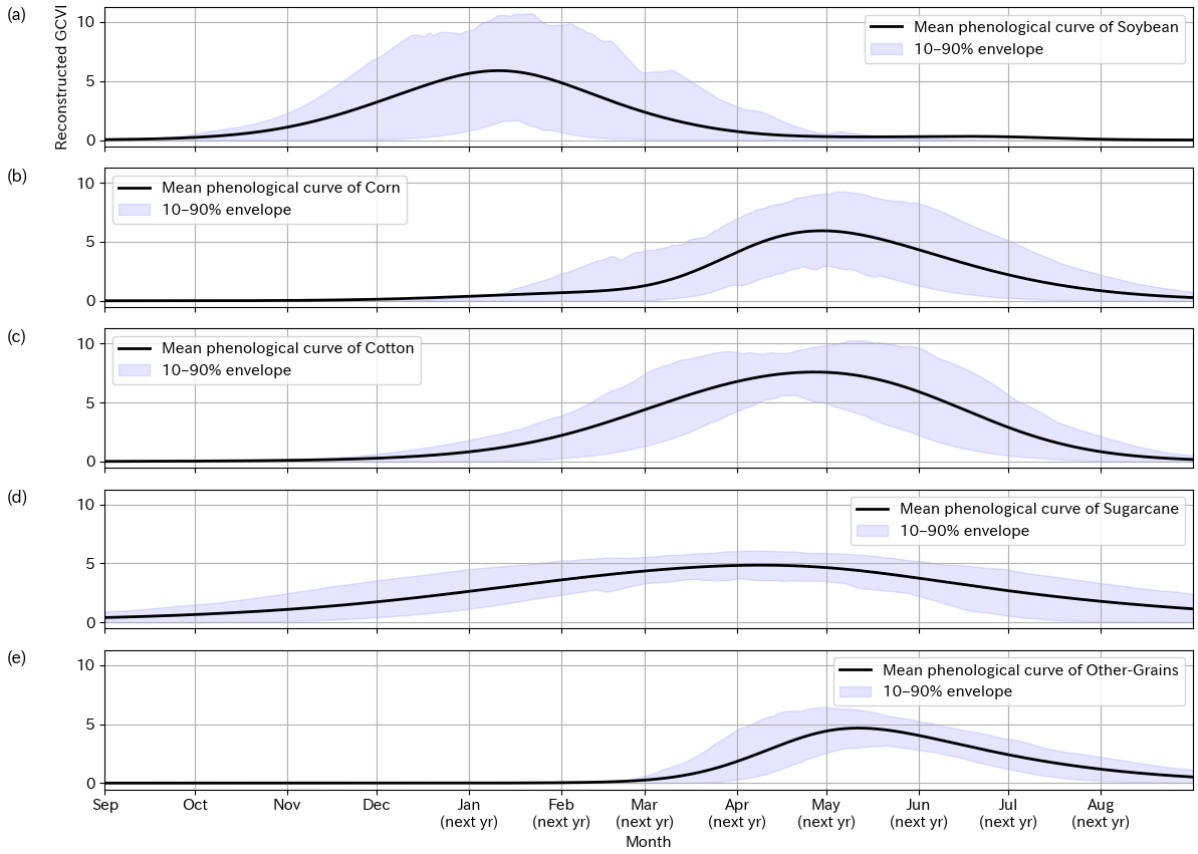

Figure 3. The extracted crop-phenology pattern of the five-target crops. (a) Soybean. (b) Corn. (c) Cotton. (d) Sugarcane. (e) Other-grains.

The crop-growing phenology and additional parameters are summarized in Figure 4. Differences in crop phenology are clearly visible in the scatter plots of the phenology-related parameters shown in Figure 4 (a)–(e). For example, the parameter ξ, which represents the relative timing of the crop phenology, is less than 0.5 (i.e., closer to September) for soybean, while other crops exhibit values greater than 0.5 (i.e., closer to the following August). In addition to the phenological parameters, topographic features indicate that sugarcane cultivation is concentrated in lower-elevation areas compared to other crops. The ALOS-2 backscatter coefficients, expressed in digital numbers (DN), also revealed clear variations among crop types. A notable example is the average ALOS-2 HH polarization value during the February–August season for corn, which is higher than that of cotton and other-grain classes. Since both cotton and other grains are also planted during the dry season, this difference in HH backscatter improves the separability of these crops.

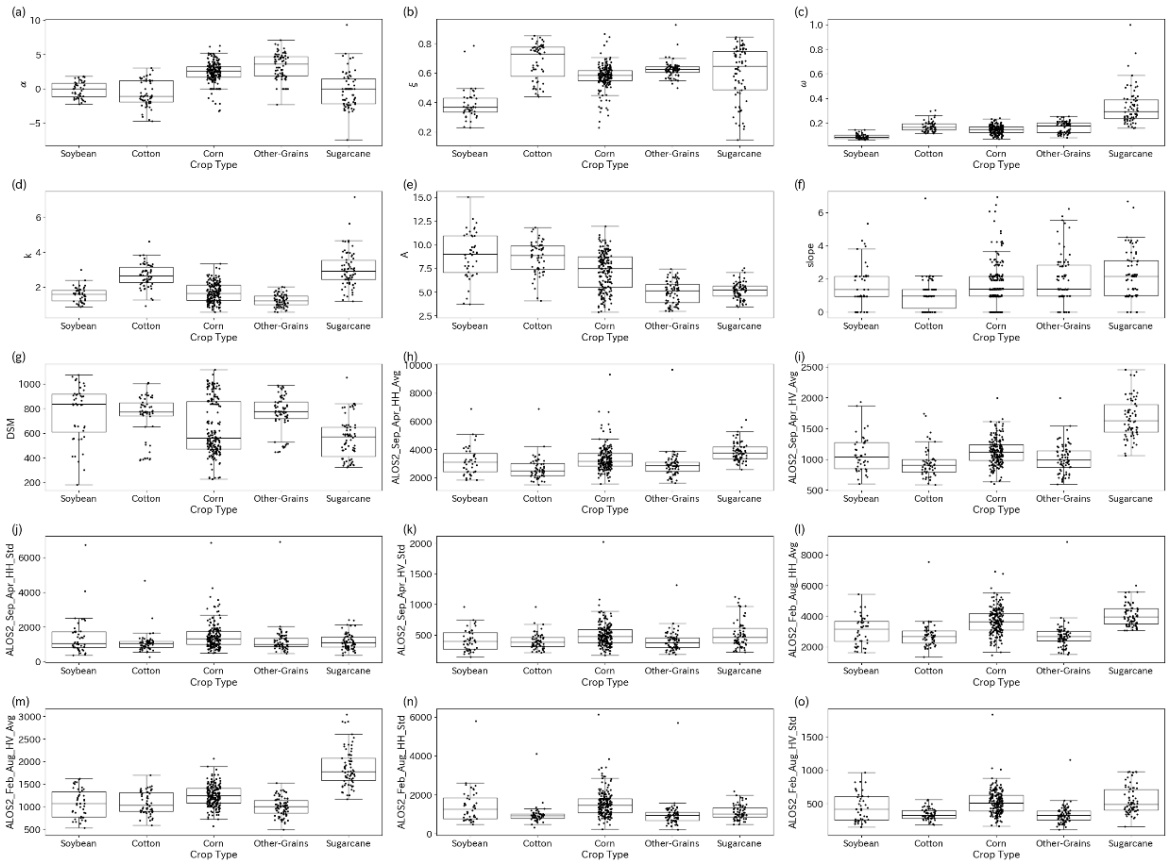

Figure 4. The distribution of the parameters of different crop-types. ALOS-2 backscatter values are DN. (a) ~ (e) Crop phenology related parameters. (f) ~ (g) Topographic features. (h) ~ (o) The ALOS-2 back-scatter statistics.

3.2 Accuracy assessment of the crop-mapping model

The model was trained on the training dataset, and the validation metrics are summarized in Table 1. Overall, the target crops were well separated from each other. Sugarcane achieved perfect classification accuracy, likely due to its distinct characteristic of a much longer growth period compared to the other crops. A few misclassifications were observed, where cotton, other grains, and soybean were occasionally classified as corn. However, the overall separability of the crops was high, supported by the combination of phenological parameters, topographic features, and ALOS-2-derived statistical variables.

Table. 1. Confusion matrix of the crop-type classification result

		Predicted					
		Corn	Cotton	Other Grains	Soybean	Sugarcane	Recall
Reference	Corn	47	0	0	1	0	0.979
	Cotton	2	12	1	0	0	0.800
	Other Grains	2	0	16	0	0	0.889
	Soybean	1	0	0	10	0	0.909
	Sugarcane	0	0	0	0	17	1
	Precision	0.904	1.000	0.941	0.909	1.000	OA= 0.936

The feature importance values of the trained model are summarized in Figure 5. It should be noted that potential multicollinearity among the variables could affect the interpretability of these importance scores. The five phenology-related parameters ranked highest among the 15 input features, indicating that the targeted crops—soybean, corn, cotton, sorghum and millet, and sugarcane—are primarily distinguished by differences in their phenological patterns. Additional parameters, such as topographic features and L-band backscatter coefficients, also contributed to improving the separability of crops with similar phenological characteristics, reflecting differences in factors such as elevation and the physical orientation of plant stems and leaves.

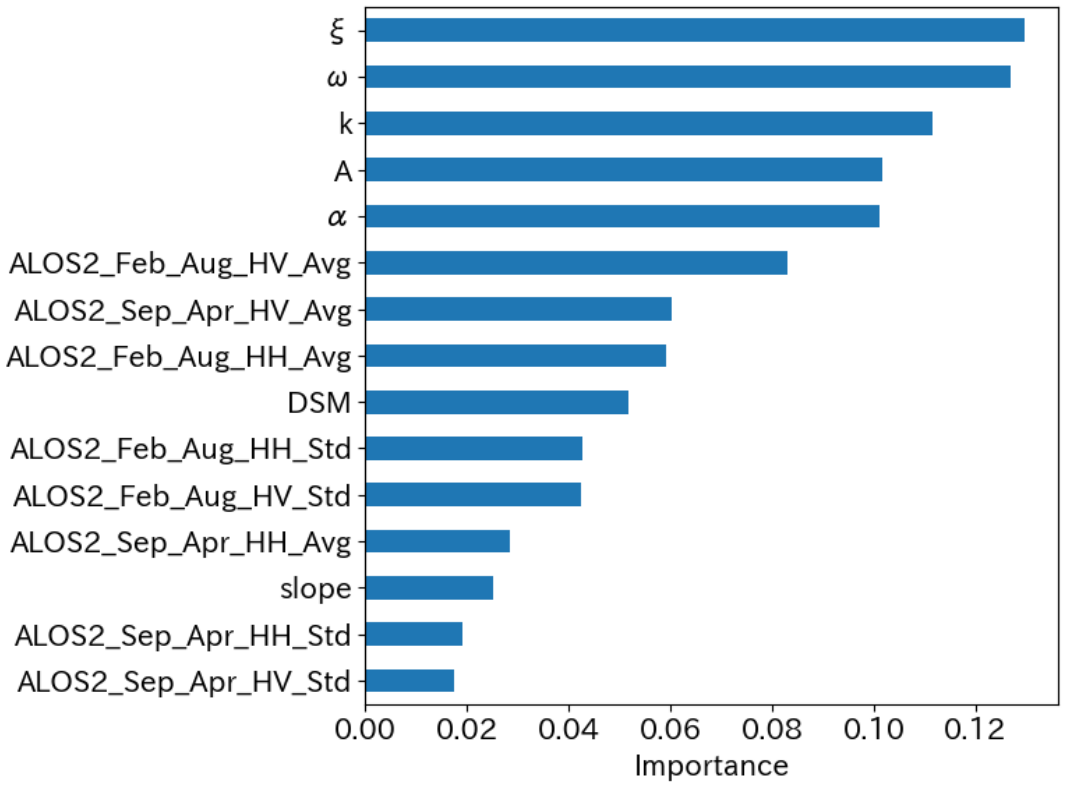

Figure 5. The feature importance values of the trained random forest model.

3.3 Crop-map generation in the central Brazilian states

The trained Random Forest model was applied to the September 2023 to September 2024 data, and the crop maps were generated at 250 m spatial resolution, as shown in Figure 6. The heterogeneous crop patterns across the region are clearly visible. During the crop-growing season, most areas are planted with either soybean or sugarcane, while corn dominates other regions, and cotton-planted areas are concentrated in the western part of Mato Grosso and parts of Bahia. Sugarcane fields are generally not used for second crops, which is consistent with the longer growth period required for sugarcane, leaving no suitable time window for additional planting.

The phenology-based approach effectively captured the mixed landscape of single- and double-cropping practices across multiple states at the pixel level, without requiring explicit prior specification of the crop-growing seasons. This represents an advantage over previous approaches for mapping temporal crops in Brazil, where the study period was manually divided into two fixed seasons.

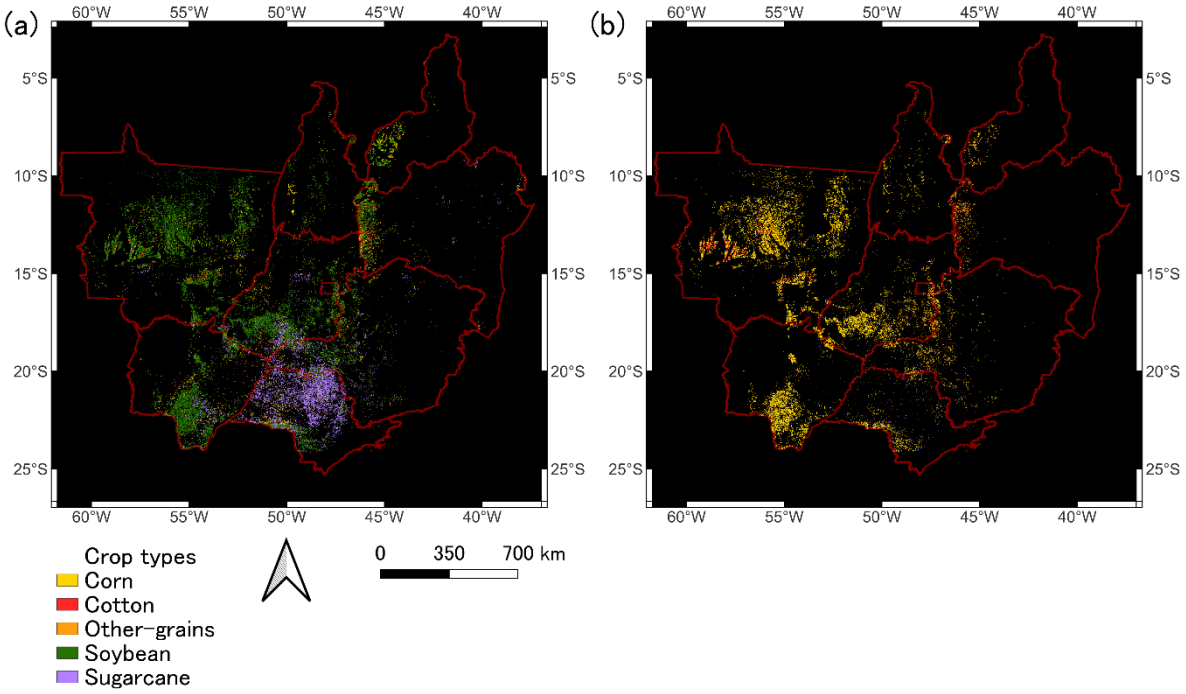

Figure 6. The crop-maps of the target region. (a) The first-season crop map. (b) The second-season crop map.

To demonstrate the benefits of the intra-annual crop-mapping strategy for capturing double-cropping practices in Brazil, a comparison with the annual land-cover map is presented in Figure 7. Figure 7(a) shows the 2023 annual MapBiomas crop map for the western Mato Grosso region. Figure 7(b) illustrates the crop map of the first crop-growing season from September 2023 to August 2024, which largely corresponds to the soybean season in double-cropping areas and is consistent with the soybean extent in the MapBiomas dataset.

The advantage of explicitly considering the second crop-growing season is highlighted in Figure 7(c), where large areas planted with corn and cotton are revealed—patterns that are not represented in the annual land-cover map in Figure 7(a). Furthermore, the current MapBiomas dataset does not classify corn as a distinct category. Therefore, the crop maps produced in this study, combined with the time-series analysis and machine-learning framework, can complement existing annual crop maps by providing enhanced information on multi-season cropping practices.

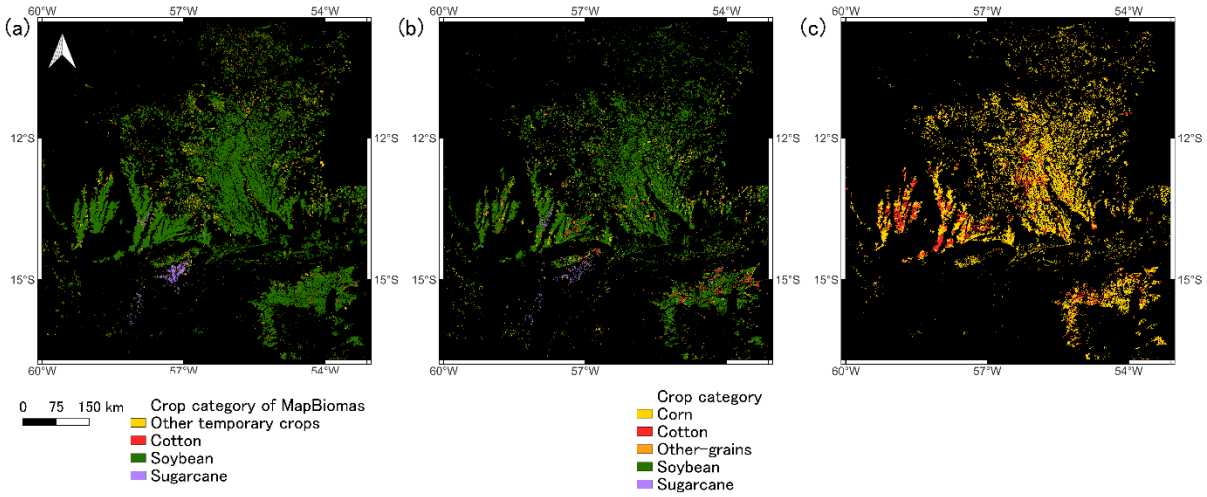

Figure 7. Comparison of the annual land-cover map in Brazil, and the multi-crop map of the current study. (a) 2023 temporary crop-map category map of the MapBiomas dataset. (b) The crop map of the first growing segment of the region from 2023/9 ~ 2024/8. (c) The crop map of the second growing segment of the region from 2023/9 ~ 2024/8.

3.4 Validation of the crop-map against the official crop-statistics

The total areas of each crop were calculated within municipalities (N = 2,745), and the results from the remote-sensing-derived crop map and the official planted area statistics from the IBGE database are summarized. Since a detailed millet production map is not publicly available, the other-grains category was excluded from this comparison.

The quantitative comparison between the remote-sensing-based crop area estimates and the official crop area statistics is shown in Figure 7. The R-squared values exceeded 0.95 for soybean, corn, and cotton, while sugarcane showed a slightly lower value of around 0.85. Overall, the municipality-level estimates demonstrated a high level of agreement between the official statistics and the remote-sensing-derived values.

However, both soybean and sugarcane estimates exhibited slight underestimation in states with extensive soybean cultivation. Since each valid cropland pixel was classified into one of the five categories, overestimation was not observed, and the contribution of the other-grains category was relatively minor compared to the major crops, this underestimation trend may be attributed to the crop mask used in this study. While the globally available Dynamic World land-cover dataset was utilized, a locally optimized land-cover dataset, such as MapBiomas, would likely be more suitable for accurately applying crop masks in future studies.

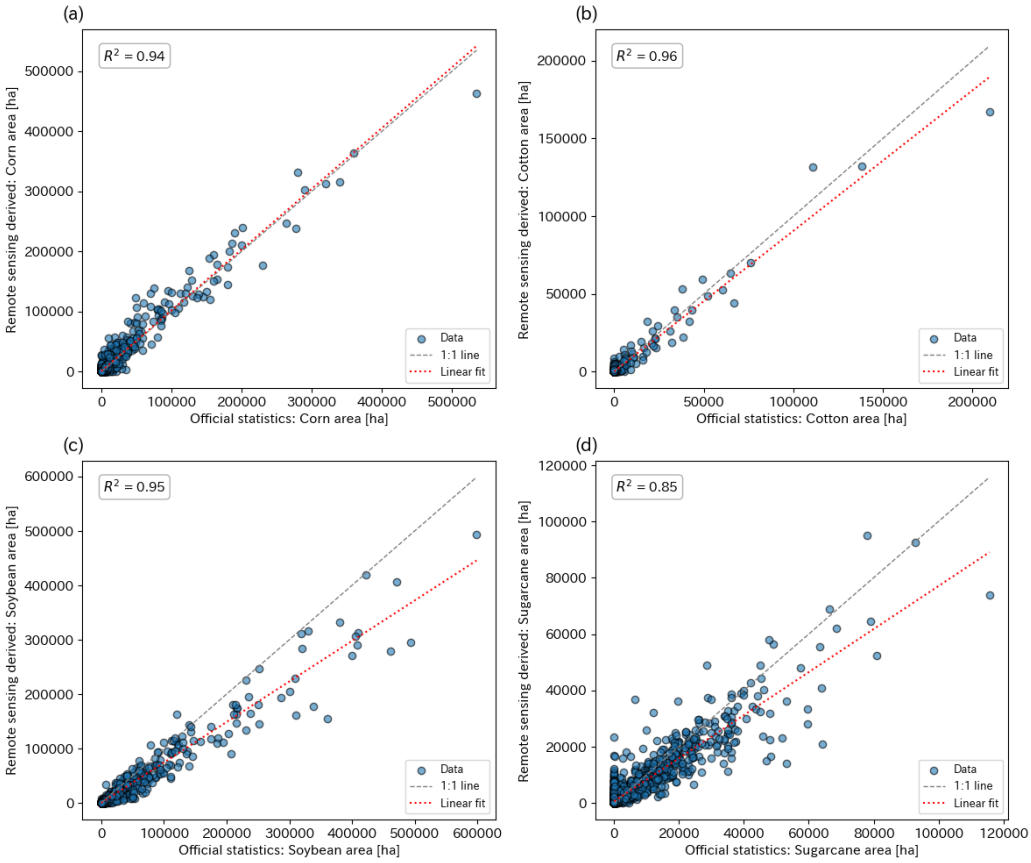

Figure 7. The comparison of the municipality-level crop planted areas. (a) Corn. (b) Cotton. (c) Soybean. (d) Sugarcane.

The remote-sensing-derived crop map successfully captured important spatial heterogeneity in crop production patterns and showed good consistency with the official statistics. Soybean-planted areas, shown in Figure 8(e) and (f), are concentrated in both the eastern and western parts of the region, particularly in the northwestern state of Mato Grosso and the eastern state of Bahia. In contrast, the corn production areas shown in Figure 8 (a) and (b) are less intensive in the eastern states compared to the western states.

Brazil's rapid corn production growth has been largely driven by the expansion of double-cropping practices in soybean-planted areas, enabling the export of corn during the United States' winter season. Therefore, accurately quantifying corn production in Brazil inherently requires addressing double-cropping systems, and crop maps must be generated separately for multiple crop-growing seasons.

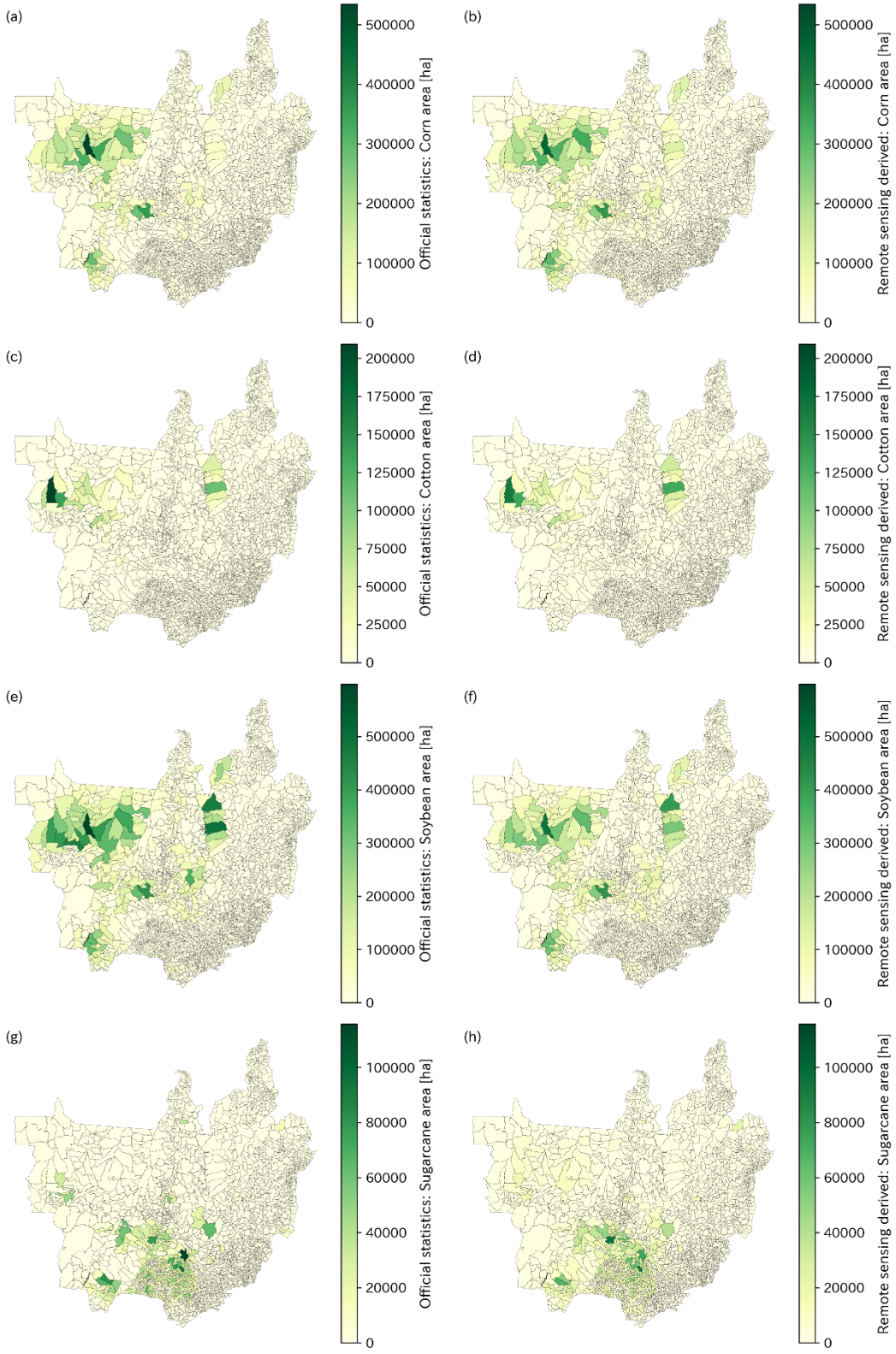

Figure 8. The official crop-area statistics, and the remote-sensing derived in central Brazilian states. The left column is the official crop-area statistics, and the right column is the remote-sensing derived crop-area statistics. (a) & (b): Corn, (c) & (d): Cotton, (e) & (f): Soybean, and (g) & (h): Sugarcane.

3.5 Future works

This study demonstrated the potential of combining multi-sensor satellite time-series data with phenology-based parameterization for crop mapping in regions with mixed single- and double-cropping systems. However, several aspects require further investigation to enhance the applicability and scalability of the approach.

First, while the current workflow successfully produced accurate crop maps, the processing of the target area at 250 m spatial resolution required approximately 2.5 hours. Timely crop monitoring at higher spatial resolutions will demand further improvements in computational efficiency. Optimizing the workflow and leveraging cloud-computing platforms such as Google Earth Engine will be essential to enable large-scale, near-real-time applications. Second, the key strength of this method lies in the extraction of crop-phenology parameters from satellite time-series data. Future work should further refine the parameterization to better handle crops with growth cycles extending beyond a single year, such as sugarcane. Since the current framework assumes that crop cycles fit within an annual period, adapting the method to accommodate multi-year phenological patterns will improve its versatility and accuracy. Finally, to ensure operational utility, the temporal consistency of the method needs to be assessed. Extending the analysis to multi-year datasets will allow evaluation of the stability and reliability of the classification across varying climatic and cropping conditions, which is critical for practical, long-term crop monitoring.

4. Conclusion

This study developed an efficient framework for mapping major crops in central Brazil's mixed single- and double-cropping systems by integrating multi-sensor satellite time-series data, phenology-based parameterization, and machine learning. Using GCVI time-series from Landsat-8/9 and Sentinel-2 with additional topographic and ALOS-2 backscatter features, the Random Forest model achieved an overall accuracy of 82.6% and showed strong agreement with municipality-level statistics ($R^2 > 0.95$ for soybean, corn, and cotton). The approach effectively captured multi-season cropping patterns without requiring prior crop calendar information and improved representation of second-season crops often missing from annual land-cover products. Future work should focus on enhancing computational efficiency, refining parameterization for long-cycle crops such as sugarcane,

and evaluating temporal consistency over multiple years to enable operational crop monitoring at higher resolutions.

Acknowledgement

During the preparation of this work the author used ChatGPT in order to improve the grammatical quality of the manuscript. After using this tool/service, the author reviewed and edited the content as needed and takes full responsibility for the content of the publication.

References

Ajadi, O. A., Barr, J., Liang, S.-Z., Ferreira, R., Kumpatla, S. P., Patel, R., & Swatantran, A. (2021). Large-scale crop type and crop area mapping across Brazil using synthetic aperture radar and optical imagery. *International Journal of Applied Earth Observation and Geoinformation*, *97*, 102294. https://doi.org/10.1016/j.jag.2020.102294

Boryan, C., Yang, Z., Mueller, R., & Craig, M. (2011). Monitoring US agriculture: the US Department of Agriculture, National Agricultural Statistics Service, Cropland Data Layer Program. *Geocarto International*, *26*(5), 341–358. https://doi.org/10.1080/10106049.2011.562309

d'Andrimont, R., Verhegghen, A., Lemoine, G., Kempeneers, P., Meroni, M., & van der Velde, M. (2021). From parcel to continental scale – A first European crop type map based on Sentinel-1 and LUCAS Copernicus in-situ observations. *Remote Sensing of Environment*, *266*, 112708. https://doi.org/10.1016/j.rse.2021.112708

Earth Observation Team of the Science and Technology Branch. (n.d.). *Agriculture and Agri-Food Canada Annual Crop Inventory*. Retrieved June 17, 2025, from https://developers.google.com/earth-engine/datasets/catalog/AAFC_ACI#description

IBGE. (2023). *PAM - Municipal Agricultural Productio*. https://www.ibge.gov.br/estatisticas/economicas/agricultura-e-pecuaria/9117-producao-agricola-municipal-culturas-temporarias-e-permanentes.html?=\&t=resultados

Khosravi, I. (2025). Advancements in crop mapping through remote sensing: A comprehensive review of concept, data sources, and procedures over four decades. *Remote Sensing Applications: Society and Environment*, *38*, 101527. https://doi.org/10.1016/j.rsase.2025.101527

Mingwei, Z., Qingbo, Z., Zhongxin, C., Jia, L., Yong, Z., & Chongfa, C. (2008). Crop discrimination in Northern China with double cropping systems using Fourier analysis of time-series MODIS data. *International Journal of Applied Earth Observation and Geoinformation*, *10*(4), 476–485. https://doi.org/10.1016/j.jag.2007.11.002

Pazhanivelan, S., Kumaraperumal, R., Vishnu Priya, M., Rengabashyam, K., Shankar, K., Nivas Raj, M., & Yadav, M. K. (2025). Multi-Temporal Analysis of Cropping Patterns and Intensity Using Optical and SAR Satellite Data for Sustaining Agricultural Production in Tamil Nadu, India. *Sustainability*, *17*(4), 1613. https://doi.org/10.3390/su17041613

Schneider, M., Schelte, T., Schmitz, F., & Körner, M. (2023). EuroCrops: The Largest Harmonized Open Crop Dataset Across the European Union. *Scientific Data*, *10*(1), 612. https://doi.org/10.1038/s41597-023-02517-0

Shimada, S., & Oyoshi, K. (2025). *Satellite-Derived Phenological Parameterization and Classification Framework for Joint Crop Intensity and Type Mapping*. https://doi.org/10.2139/ssrn.5402822

Sota, H., Takeo, T., Masato, O., Yousei, M., Kenlo, N. N., Koichi, I., Naoyoshi, H., Fumi, O., Masanori, D., & Tsutomu, Y. (2022). Generation of High-Resolution Land Use and Land Cover Maps in JAPAN Version 21.11. *Journal of The Remote Sensing Society of Japan*, *42*(3), 199–216.

Souza, C. M., Z. Shimbo, J., Rosa, M. R., Parente, L. L., A. Alencar, A., Rudorff, B. F. T., Hasenack, H., Matsumoto, M., G. Ferreira, L., Souza-Filho, P. W. M., de Oliveira, S. W., Rocha, W. F., Fonseca, A. V., Marques, C. B., Diniz, C. G., Costa, D., Monteiro, D., Rosa, E. R., Vélez-Martin, E., … Azevedo, T. (2020). Reconstructing Three Decades of Land Use and Land Cover Changes in Brazilian Biomes with Landsat Archive and Earth Engine. *Remote Sensing*, *12*(17), 2735. https://doi.org/10.3390/rs12172735

Tatsumi, K., Yamashiki, Y., Canales Torres, M. A., & Taipe, C. L. R. (2015). Crop classification of upland fields using Random forest of time-series Landsat 7 ETM+ data. *Computers and Electronics in Agriculture*, *115*, 171–179. https://doi.org/10.1016/j.compag.2015.05.001

Wang, S., Azzari, G., & Lobell, D. B. (2019). Crop type mapping without field-level labels: Random forest transfer and unsupervised clustering techniques. *Remote Sensing of Environment*, *222*, 303–317. https://doi.org/10.1016/j.rse.2018.12.026

Wang, S., Di Tommaso, S., Deines, J. M., & Lobell, D. B. (2020). Mapping twenty years of corn and soybean across the US Midwest using the Landsat archive. *Scientific Data*, *7*(1), 307. https://doi.org/10.1038/s41597-020-00646-4

WorldMeter. (n.d.). *World Population*. Retrieved September 11, 2025, from https://www.worldometers.info/world-population/#:~:text=World%20Population%20Clock%3A%208.2%20Billion,(LIVE%2C%202025)%20%2D%20Worldometer